Am J Clin Exp Urol 2022;10(6):425-439
www.ajceu.us /ISSN:2330-1910/AJCEU0148515

Original Article

Single-cell RNA-Seq identifies factors necessary for the regenerative phenotype of prostate luminal epithelial progenitors

Daniel C Moline[1], Morgan L Zenner[2], Alex Burr[2], Jordan E Vellky[2], Larisa Nonn[2], Donald J Vander Griend[2]

[1]*Committee on Development, Regeneration, and Stem Cell Biology (DRSB), The University of Chicago, Chicago, IL 60612, USA;* [2]*Department of Pathology, The University of Illinois at Chicago, Chicago, IL 60612, USA*

Received December 14, 2022; Accepted December 23, 2022; Epub December 25, 2022; Published December 30, 2022

Abstract: Benign prostate hyperplasia and prostate cancer are common diseases that involve the overgrowth of prostatic tissue. Although their pathologies and symptoms differ, both diseases show aberrant activation of prostate progenitor cell phenotypes in a tissue that should be relatively quiescent. This phenomenon prompts a need to better define the normal prostate progenitor cell phenotype and pursue the discovery of causal networks that could yield druggable targets to combat hyperplastic prostate diseases. We used single-cell (sc) RNA-Seq analysis to confirm the identity of a luminal progenitor cell population in both the hormonally intact and castrated mouse prostate. Using marker genes from our scRNA-Seq analysis, we identified factors necessary for the regeneration phenotype of prostate organoids derived from mice and humans *in vitro*. These data outline potential factors necessary for prostate regeneration and utilization of scRNA-Seq approaches for the identification of pharmacologic strategies targeting critical cell populations that drive prostate disease.

Keywords: Prostate, single-cell RNA-Seq, regeneration, luminal progenitor cells, BCL-2, HIPPO signaling, prostate organoids, prostate stem cells, prostate progenitor cells

Introduction

The prostate is an accessory sex organ located beneath the bladder that is responsible for secreting prostatic fluid [1-3]. This organ has a high rate of neoplastic and hyperplastic disease, with prostate cancer being among the most common cancers in men, and benign prostate hyperplasia (BPH) affecting a majority of men over the age of 60 [4-6]. One mechanism proposed to underlie this high rate of prostatic disease is aberrant prostate epithelial progenitor activity [7-9]. However, our knowledge of these epithelial progenitors remains limited. Better understanding these cells, particularly both their biomarkers and the pathways necessary for their regenerative phenotype, may provide significant insight and pharmacologic strategies to target the initiation and progression of prostate disease.

Mice provide a tractable model system for studying prostate epithelial progenitors due to their capacity for hormone-dependent regeneration. After castration, the mouse prostate undergoes a wave of apoptosis, shrinking to approximately one-tenth its original size [10-13]. Reintroduction of androgen, often through surgical implantation of a testosterone pellet, regenerates the prostate and recapitulates its original ductal architecture and secretory function [10, 11]. This hormonal modulation of progenitor cell regenerative activity allows direct investigation of cells in the prostate epithelium that possess the capacity for glandular regeneration, enabling identification of optimal factors for targeted treatment. Using this model, researchers have found that mouse prostate regeneration is partially dependent upon the regenerative activity of cells located proximal to the urethral ducts and referred to as prostate epithelial progenitor cells [14]. Originally thought to only belong to the basal epithelial lineage, cells demonstrating regenerative capacity *in vivo* also have been reported in the luminal

compartment of the prostate epithelium [7]. A rare subset of luminal epithelial cells also is bipotent when cultured as organoids in vitro [14]. Additionally, single-cell transcriptomics have identified numerous biomarkers for the luminal progenitor cell (LPC) population [15, 16].

Similar single-cell transcriptomic approaches can enable identifying candidate pathways and factors necessary for the regenerative phenotype in an unbiased way. Here, we used single-cell RNA-sequencing (scRNA-Seq) data to analyze the intact and castrate prostate, quantifying the change in biomarkers after loss of androgen as well as identifying candidate pathways for progenitor cell ablation. These candidate pathways were chemically perturbed using *in vitro* organoid cultures of cells derived from mice as well as human patients to determine the necessity of these signaling pathways for regeneration and growth. These data provide new information on the behavior of prostate progenitor cells as well as unique candidates for future therapeutic targeting of prostate progenitor cells in disease states.

Methods

Single-cell RNA-Seq analyses of mouse prostate tissue

Acquisition and analyses of all animal tissues were conducted in accordance with institutional guidelines and an IACUC-approved protocol. C57Bl6 mice were obtained from Harlan/Envigo (Indianapolis, IN) and castrated according to institutional guidelines at 8 weeks of age. A cohort of castrated mice was subcutaneously implanted with a 1.0-cm silastic implant packed with powdered testosterone (Steraloids, Newport, RI) and sealed with silicone adhesive, providing a "hormone normal" condition [17]. Another cohort of mice were left without a testosterone implant, providing a "castrate" condition. After 3 weeks, mice were euthanized according to institutional guidelines before prostate removal and dissection.

Dissected prostate lobes were dissociated enzymatically using type I collagenase (Sigma-Aldrich, St. Louis, MO) and dispase (STEMCELL Technologies, Vancouver, Canada). The resulting single-cell solution was counted using a cellometer (Nexcelom, Lawrence, MA). Using a threshold of 70% cell viability, viable samples were processed using our previously reported 10X 3' scRNA-Seq V2 protocol [18]. Briefly, cells were separated into individual microfluidic droplets along with an oligonucleotide-covered gel bead using the 10X Chromium Controller (10X Genomics, Pleasanton, CA). Cells were lysed in the presence of their respective beads to capture their transcripts. Captured transcripts were converted to cDNA and eventually into an Illumina-compatible sequencing library according to the 10X protocol. The resulting library was sequenced at the University of Illinois at Urbana-Champaign on an Illumina NovaSeq (Illumina, San Diego, CA) at 100-bp paired-end read depth. Reads were aligned to the mm10 annotated reference genome using CellRanger v3.0.1 (10X Genomics). Quality control and clustering were performed in the R Package Seurat (Satija Lab, New York, NY) [19]. Downstream pathway analysis was performed with Ingenuity Pathway Analysis (IPA) (Qiagen, Hilden, Germany).

Mouse and human organoid culture and colony forming unit assays

Prostates from three intact mice 8-12 weeks of age were enzymatically dissociated using type II collagenase (Sigma-Aldrich) and dispase (STEMCELL Technologies). The resulting single-cell solution was re-suspended in 50% growth factor-reduced, phenol red-free Matrigel (Corning, Corning, NY) and plated in serum-free advanced DMEM (Thermo Fisher Scientific, Waltham, MA) containing A83-01 (A.G. Scientific, San Diego, CA), y-27632 (STEMCELL Technologies), R-Spondin (Peprotech, Rocky Hill, NJ), and Noggin (Peprotech, Rocky Hill, NJ) at previously published concentrations [20]. Mouse organoids were plated into six technical replicates per treatment condition for each biological replicate. Small molecule inhibitors were administered upon plating of the organoids, and treatment proceeded for 72 h before imaging wells on a Keyence BZ-X800 microscope (Keyence, Osaka, Japan). Wells were imaged at 4x magnification, acquiring a 3D Z-stack of the entire well. Max projection images were created from the Z-stacks, allowing viewing of all organoids in one 2D image. Stitched images were counted using the automated cell counting function in the Keyence Image Analysis software. To ensure counting of organoids specifically and not individual cells or small cell

clumps, a perimeter size threshold of ≥ 200 μm was used for analysis. This threshold yielded counting results that most closely mirrored preliminary hand-counted results, calibrating the software to the researcher's definition of an organoid according to size and circularity. Organoid counts from individual wells were then divided by the total number of cells plated in that well, yielding a percentage of colony forming units (CFU) that could be used as a rough measurement of regenerative capacity. Percentage of CFU data were compared using a two-tailed student's t-test with a significance threshold of $t < 0.05$.

Human organoid culture was performed using a previously published protocol detailed in McCray et al. 2019 [18]. Briefly, biopsies obtained using IRB-approved guidelines from healthy regions of human prostates were dissociated into single cells and cultured as 2D prostate epithelial cells before being transferred to 3D culture in 33% Matrigel and fed with KSFM media (Thermo Fisher Scientific). Human organoids were treated with drugs upon plating and imaged as previously described [18]. CFU were also determined and compared between treatment conditions in the same manner as mouse organoid assays.

Flow sorting and organoid culture of dissociated mouse prostates

Prostates from mice 8-12 weeks of age were dissociated using collagenase and dispase. The resulting single-cell solution was stained with conjugated antibodies targeting CD26 (FITC) and TSPAN8 (PE) (Supplementary Table 1). Samples were sorted on a MoFlo Astrios (Beckman Coulter Life Sciences, Indianapolis, IN) at the University of Illinois Chicago Flow Cytometry Core. The resulting sorted cells were re-suspended in 100% Matrigel and cultured similarly to our mouse organoid experiments detailed above. A higher percentage of Matrigel was used to improve initial survival for cells after the stress of flow sorting. Wells were imaged using the Keyence BZ-X800, and the number of organoids per well was divided by the number of cells plated initially to give a percentage of CFU for each sorted fraction. Statistical significance was determined using a two-tailed t-test.

Imaging of mouse tissue sections and organoids

Prostates from three castrated and hormone intact 11-week-old mice were dissected and cryoembedded in OCT (Sakura Finetek, Nagano, Japan). Cryoembedded prostates were cut and placed on slides by the University of Illinois at Chicago Research Histology and Tissue Imaging Core. Sections were stained using primary and secondary antibodies at concentrations detailed in Supplementary Table 1. Stained slides were imaged on a Keyence BZ-X800 microscope. Images were analyzed using the accompanying Keyence Image Analysis software as well as FIJI. Images were adjusted for exposure and haze reduction using corresponding functions in the Keyence Image Analysis software and subsequently counted using a cell counting macro in FIJI. Three biological replicates were used for each staining, with four technical replicates within each biological replicate. Images provided in figures are representative of fluorescent staining observed in all biological replicates.

Statistical analyses

Statistical analyses were performed in R. Statistical tests for our scRNA-Seq dataset were performed using the Seurat add-on for R, and any reported *p*-values referring to scRNA-Seq expression are adjusted *p*-values that account for multiple sampling errors. These adjusted *p*-values are supplied by the program's clustering algorithm, which is thoroughly explained by Butler et al. [21]. In our organoid drug treatment experiments, conditions were compared to one another using a two-tailed student's t-test with a threshold of $P < 0.05$. This analysis was performed using each of the six technical replicates as the dataset for the specific experimental condition, and the analysis was performed within each biological replicate for that particular drug experiment. Biological replicates were not compared directly to one another in an effort to avoid the confounding effects of stochastic differences in regenerative potential between individual replicates. A similar approach was undertaken with the human organoid drug treatment conditions, with each drug treatment compared to the vehicle condition (DMSO alone) using a two-tailed t-test with a threshold of $t < 0.05$.

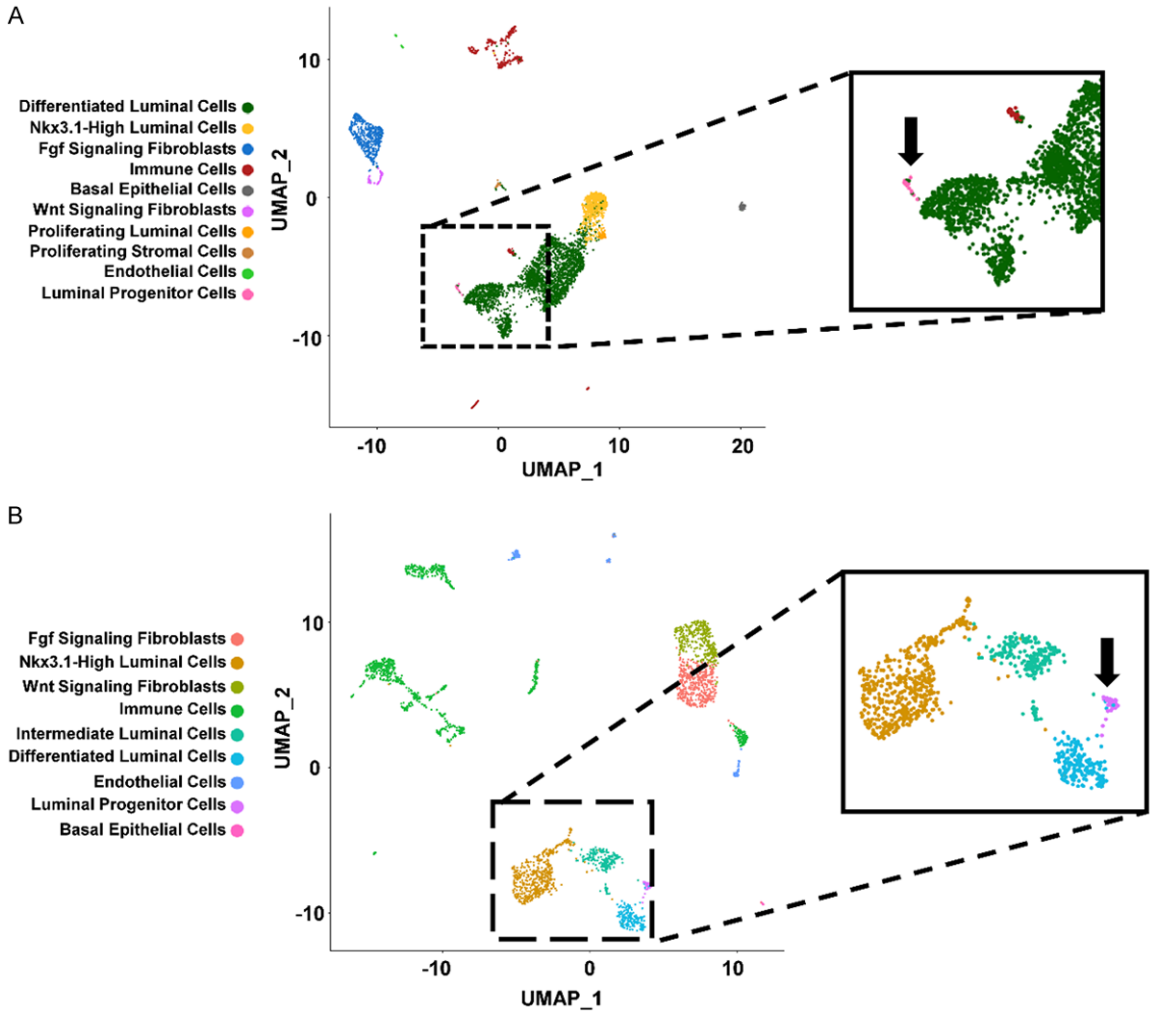

Figure 1. scRNA-Seq Uniform Manifold Approximation and Projection (UMAP) with Identified Cell Populations. A. UMAP for intact prostate depicting identified populations. B. UMAP for castrate prostate depicting identified populations.

Results

scRNA-Seq analyses of castrate and intact mouse prostates

We investigated unique cell populations of the mouse prostate to catalog their biomarkers and potential critical signaling pathways as well as to discern key changes to cellular composition and signaling during castration. We used single-cell RNA-Seq analysis of cells from both intact and castrate prostates of mice 8-12 weeks of age (see Supplementary Table 2 for cell sample quality). Raw expression matrices from these data were run through a quality-control workflow in Seurat, an R add-on used for dimensional reduction-based analysis of scRNA-Seq datasets [21]. Our quality-control workflow enabled removal from the dataset of cells with too few reads (indicating they were poorly captured), too many reads (indicating a doublet of two cells was captured), or > 10% of mitochondrial reads (indicating cells were dead or dying). This curated dataset was then subjected to dimensional reduction analysis, producing 17 clusters in the hormone intact condition and 18 clusters in the castrate condition. Due to the high level of diversity observed in our initial analysis, we performed a secondary supervised clustering step as well. This stage involved combining cryptically diverse clusters that have yet to be experimentally validated as well as clusters that are outside the research interests of this study, yielding supervised datasets consisting of 10 cell clusters in intact prostate (**Figure 1A**) and 9 cell clusters in castrate prostate (**Figure 1B**).

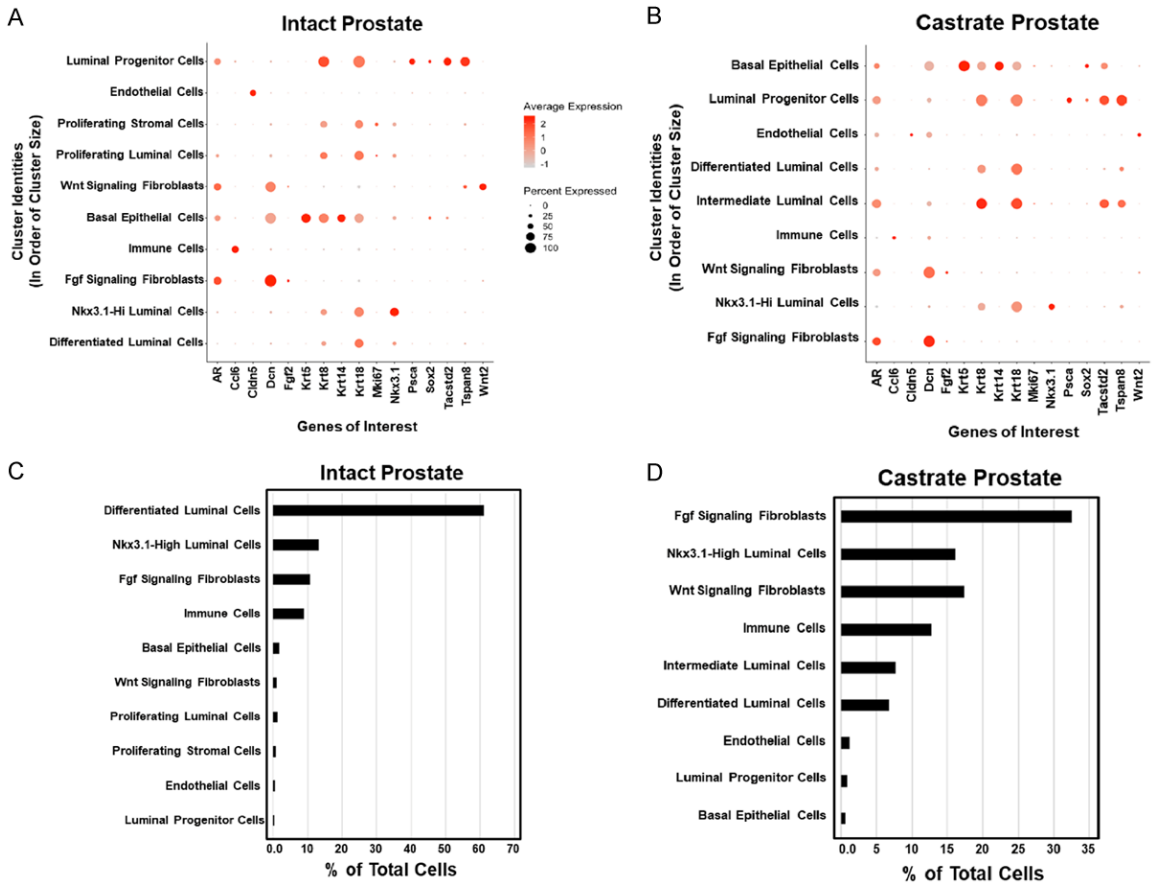

Figure 2. Expression Patterns Among Cell Populations in scRNA-Seq Data. A. Dotplot depicting expression of relevant factors in the intact prostate condition. B. Dotplot depicting expression of relevant factors in the castrate prostate condition. C. Quantity of identified populations as a percentage of total plated cells in the intact prostate sample. D. Size of identified populations as a percentage of total plated cells in the castrate prostate sample.

In the intact condition, we identified a cluster of cells expressing statistically significant biomarkers consistent with differentiated luminal cells: cytokeratin 8 (*Krt8*), cytokeratin 18 (*Krt18*), and prostate stem cell antigen (*Psca*) (**Figure 2A**). Differentiated luminal cells were 61% of total cells in the intact prostate, constituting a majority of cells in the sample (**Figures 1A** and **2C**). In addition to differentiated luminal cells, we also identified a group of luminal cells expressing high *Nkx3.1* as well as the normal luminal cell markers *Krt8* and *Krt18*, which we designated as Nkx3.1^{Hi} luminal cells. A proliferating luminal cell population detected in the intact prostate expressed *Ki67* as well as *Krt8* and *Krt18*. Although the prostate is largely considered quiescent in the hormone normal state, there is a limited rate of epithelial turnover that could account for the observed proliferating luminal cell population [22]. Another cluster of cells were labeled as putative LPCs expressed *Krt8* and *Krt18* as well as putative progenitor cell markers, including SRY-box transcription factor 2 (*Sox2*), tumor-associated calcium signal-transducer 2 (*Tacstd2, also referred to at Trop2*), and prostate stem cell antigen (*Psca*) [23-25].

Three clusters were identified due to expression of stromal fibroblast markers. One cluster of cells expressing the stromal marker decorin (*Dcn*) as well as signaling ligand fibroblast growth factor 2 (*Fgf2*) was identified as Fgf signaling fibroblasts (**Figures 1A** and **2A**, **2C**). Another signaling fibroblast cluster expressing *Dcn* as well as *Wnt2* was referred to as Wnt signaling fibroblasts. Both FGF and WNT signaling factors play a role in prostate development and epithelial regeneration [26-28]. Lastly, a group of cells expressing *Dcn* as well as *Ki67* were identified as proliferating stromal cells. We also

identified a cluster of cells that expressed numerous immune cell markers, including *Ccl6*, a marker of T-cells. Endothelial cells also were present among the stromal populations identified in the intact condition, marked by expression of *Cldn5*. As a final cluster, basal epithelial cells were identified in the intact prostate, expressing *Krt5*, *Krt14*, and progenitor cell markers including *Sox2* and *Tacstd2*. Other basal populations that were ostensibly more differentiated and did not express these progenitor cell markers were not resolved within this dataset, likely owing to underrepresentation of the cell types after tissue digestion.

Investigation of the castrate prostate identified numerous similar populations to those found in the intact prostate while also uncovering unique populations. Differentiated luminal cells were again identified, expressing *Krt8*, *Krt18*, and *Pbsn* (**Figures 1B** and **2B**, **2D**). The persistence of differentiated luminal cells in the castrate condition is interesting because these cells are considered androgen-dependent. Differentiated luminal cells are a much smaller percentage of total cells in the castrate prostate (6.8%) compared to the intact prostate (61.1%), showing some adherence to predicted androgen dependence of these cells. The small population of surviving differentiated luminal cells in the castrate prostate may express a survival program that allows them to persist in the absence of androgen, although further experimentation is necessary to test this hypothesis. Nkx3.1^{Hi} luminal cells also were identified in the castrate prostate, again expressing *Krt8*, *Krt18*, and *Nkx3.1*. An additional luminal population observed exclusively in the castrate condition expressed *Krt8*, *Krt18*, and *Tacstd2*. Interestingly, this population did not significantly express the putative progenitor markers *Psca* and *Sox2* that were observed in the LPC population in the intact condition. This led to identification of this cluster as intermediate luminal cells, although their relationship to the LPC population requires further investigation.

LPCs also were identified in the castrate condition, once again expressing *Krt8, Krt18, Sox2, Psca*, and *Tacstd2* (**Figures 1B** and **2B**, **2D**). Additionally, the proliferating luminal population was notably absent from the castrate condition, implying a lack of epithelial turnover in the absence of androgen signaling. Basal epithelial cells were observed in the castrate prostate, expressing *Krt5, Krt14, Sox2*, and *Tacstd2* similar to the intact condition. Immune cells and endothelial cells also were observed in the castrate prostate, expressing markers similar to the intact condition. Signaling fibroblasts also were observed in the castrate condition, including both Fgf signaling and Wnt signaling fibroblast populations. Importantly, however, the proliferating stromal population was absent from the castrate condition. The lack of proliferating luminal and stromal populations in the castrate condition implies that there was a lower rate of tissue turnover in the absence of androgen signaling.

Identifying and defining LPCs

LPCs are of particular interest given their role in both epithelial regeneration and disease initation [7, 15]. These cells are thought to contribute to disease initiation, yet there is little knowledge of the mechanistic contributors to their specific phenotype [7, 9]. Our comparison of intact vs. castrate conditions enabled us to establish a marker profile for murine LPCs. This profile includes *Krt8, Krt18, Psca, Tacstd2*, and *Sox2*, as these factors are expressed by the LPC population in both intact and castrate hormone conditions. These putative progenitor markers have been independently verified to enrich for progenitor cell phenotypes in the mouse prostate epithelium [23, 25, 29]. Although the LPC populations identified in the intact and castrate conditions shared numerous similarities, they also had notable differences in expression patterns. Castrate LPCs expressed certain notable factors, including the morphogen sonic hedgehog (*Shh*) and a putative progenitor cell marker lymphocyte antigen 6 family member D (*Ly6d*). Further investigation is required to understand the implications of these different expression patterns between host hormone states. Additionally, there was more than two-fold enrichment in the number of LPCs in the castrate condition (0.8%) compared to the intact condition (0.3%), in agreement with the observed enrichment of cells with a progenitor phenotype in the castrate prostate (**Figure 2B**, **2D**) [7, 16]. Overall, these data show that a suite of biomarkers corresponding to the LPC population can be identified using scRNA-Seq analysis, and that these cells can be discerned from more differentiated

luminal populations in both the castrate and intact conditions.

Immunofluorescence and flow cytometry validation of LPC biomarkers

The LPC population is of particular interest in the field of prostate regeneration, specifically at the intersection of prostate regeneration and disease [7, 15]. Although these cells have been more clearly defined as experimental methods have become more precise, the mechanistic underpinnings and therapeutic vulnerabilities of these cells are not entirely understood. The similarities between the regenerative phenotype and the behaviors exhibited by cells in neoplastic and hyperplastic disease, along with cells of a luminal identity constituting the vast majority of cells in prostate cancer, makes understanding the signaling mechanisms that contribute to LPCs' capacity for survival and regeneration an important clinical target.

We thus validated our marker suite using immunofluorescence microscopy and flow cytometry. Specifically, we were interested in validating expression patterns of the LPC population in intact and castrate conditions. This population is not only of interest due to a relative lack of study of its mechanistic underpinnings but also due to its possible role in prostate disease [7]. Immunofluorescence microscopy on cryo-embedded mouse prostates demonstrated overlap of Psca and Tspan8/Tacstd2, two significant markers for the LPC population, in both intact and castrate conditions (**Figure 3A**). Flow cytometry targeting CD26+/Tspan8+ cells showed the presence of candidate LPCs in the intact prostate at 0.5% of total live cells (**Figure 3B**). Although our flow cytometry approach yielded a higher percentage of LPCs in the dissociated prostate compared to our scRNA-Seq data, this may be due to lack of specificity in our gating approach; *Tspan8* transcript expression may be an LPC marker according to our scRNA-Seq but also may mark a small population of cells other than LPCs. Future experimentation may require inclusion of additional markers in our flow cytometry panel to avoid impurities in sorted fractions and account for the differences between *Tspan8* transcript and Tspan8 protein. Overall, these results validate the expression pattern of biomarkers identifying the LPC population in our scRNA-Seq dataset.

Pathway analysis of candidate LPCs

We next wanted to understand the factors necessary for the LPC phenotype in an effort to possibly perturb their regeneration. IPA was used to analyze gene lists generated from the LPC populations identified with scRNA-Seq from both intact and castrate conditions. The gene list was enriched for upregulation of genes associated with cell self-renewal (z-score = 2.781), cell survival (z-score = 3.631), growth of organism (z-score = 2.738), colony formation (z-score = 2.13), and colony formation of cells (z-score = 2.31) (**Figure 4A**). De-enriched gene lists with a z-score less than -2 included congenital malformation of the urogenital system (z-score = -2.936), apoptosis of epithelial cells (z-score = -2.048), morbidity or mortality (z-score = -10.444), organismal death (z-score = -10.377), and apoptosis (z-score = -3.265). Additionally, upstream regulator analysis revealed a list of factors predicted to affect the LPC phenotype, including *Yap1* (z-score = 2.449), a transcription factor in the Hippo pathway, as well as numerous upstream regulators of *Bcl-2*, a factor with anti-apoptotic activity (Supplementary Figure 1). Factors with an established role in regulating Bcl-2 that were identified by upstream analysis included positive regulators IL12 (z-score = 2.00), HIF1A (z-score = 2.027), ARNT (z-score = 2.156), MAPK9 (z-score = 3.020), and downregulation of negative regulator SATB1 (z-score = -2.121) (Supplementary Figure 1). Altogether, enrichment of factors associated with functional outputs reinforces identification of the LPC cluster as well as possible mechanistic contributors for the maintenance of these progenitor cells. In particular, our analysis prioritized multiple factors, including Yap1, Bcl-2, p38 MAP kinase, Smo, Notch1, and negative control Nf-kB (**Figure 4B**). Preliminary testing using *in vitro* murine organoid models of these candidate factors narrowed our investigation down to Yap1, Bcl-2, p38 MAP kinase, and Nf-kB (data not shown). Although these factors have been investigated in some capacity in prostate cancer, investigation in the context of normal prostate regeneration has been limited [30-33]. We therefore examined the necessity of these factors for the LPC regenerative phenotype.

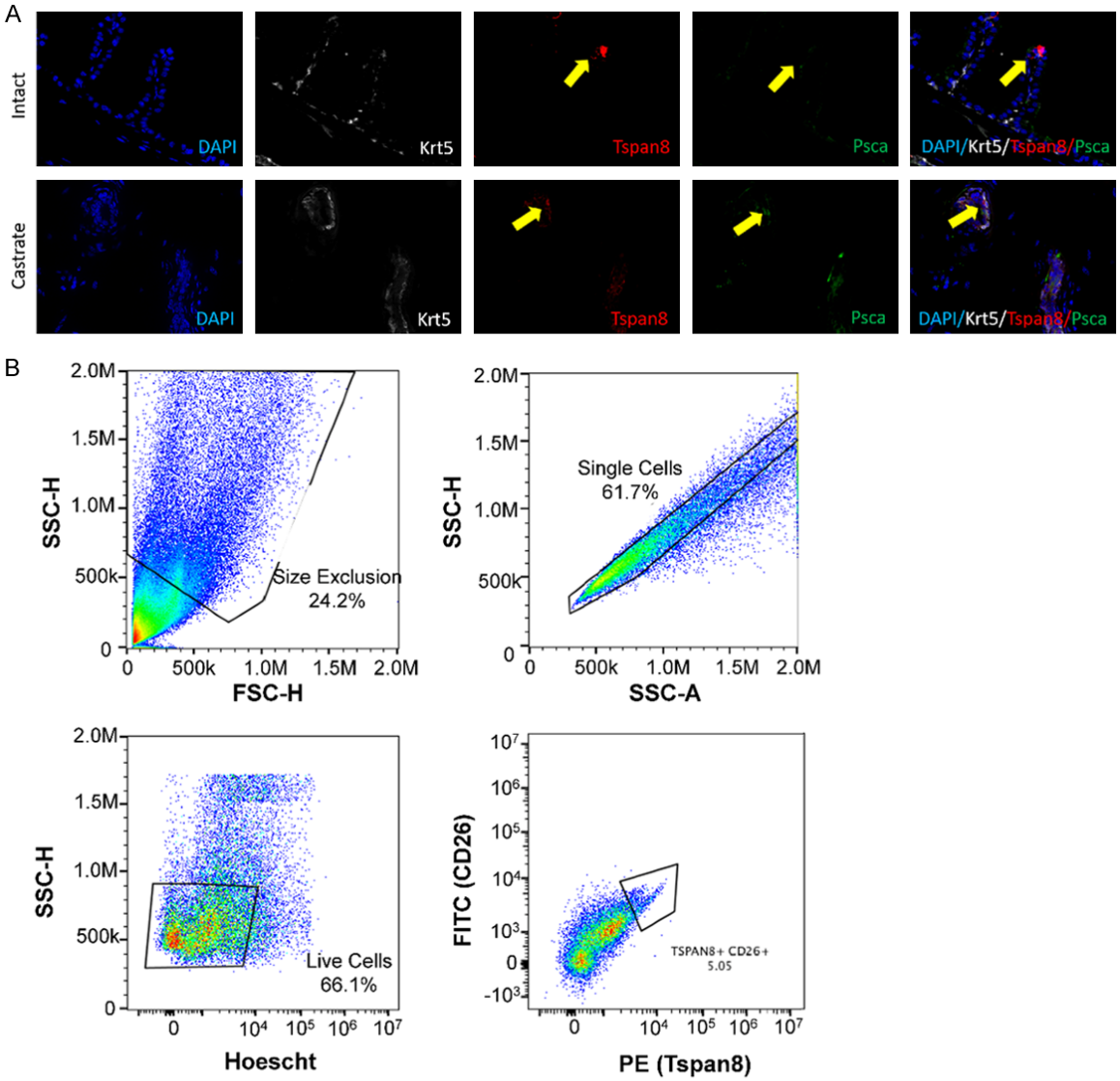

Gate	%Parent	%Total
Size Exclusion	24.20%	24.20%
Single Cells	61.70%	14.90%
Live Cells	66.10%	9.95%
Tspan8+/CD26+	5.05%	0.5%

Figure 3. Immunofluorescence and Flow Cytometry Validation of Luminal Progenitor Cell Biomarker Expression. A. Immunofluorescence data including luminal cells expressing Tspan8 and Psca (arrows) in mouse prostate tissues obtained from hormonally intact or castrated mice. B. Flow cytometry data for cells expressing both CD26 and Tspan8 from hormonally intact mouse prostate.

Small molecule inhibitors targeting LPC factors reduce the regenerative phenotype of mouse organoids

To both validate our IPA results and identify possible avenues to ablate the prostate's regenerative phenotype, we tested small molecule inhibitors targeting factors of interest using *in vitro* organoid culture. Mouse organoids were plated at 1000 cells per well in the presence of drug and allowed to grow for 72 h before being imaged and counted. Treatment with CA3, a small molecule inhibitor targeting Yap1, significantly reduced organoid growth and regeneration as evidenced by a reduced percentage of CFU compared to controls (P = 0.02, 0.004, 0.02 in biological replicates) (**Figure 5A**) [34]. These data implicate the Hippo signaling pathway in the regenerative phenotype of mouse progenitor cells *in vitro*.

A

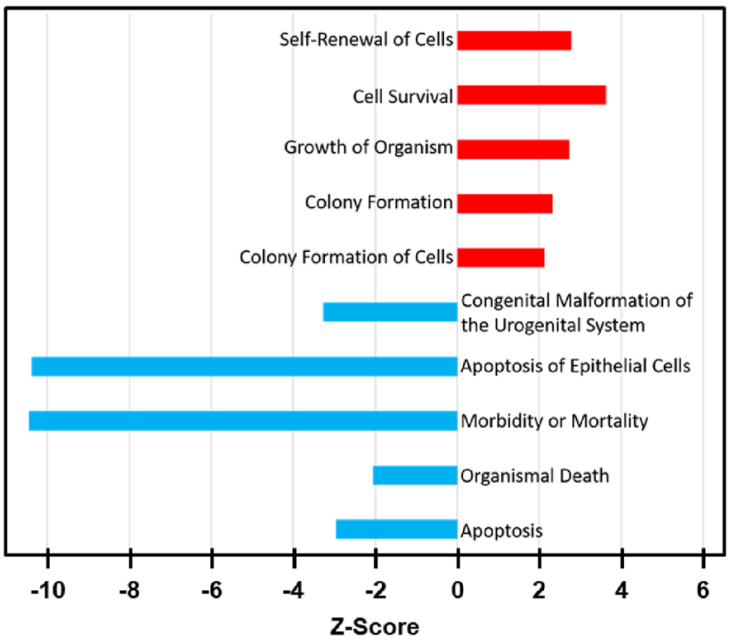

B

Factor Name	IPA-Predicted Expression	Drug
Yap1	High	CA3
Bcl2	High	Venetoclax
p38 MAPK	High	SB203580
Smo	High	XAV-939
Notch1	High	FLI-06
NF-kB *(negative control)*	Low	SC75741

Figure 4. Pathway Analysis of Luminal Progenitor Cell Expression Profile. A. Top five activated and top five deactivated diseases and functions according to Z-score generated by Ingenuity Pathway Analysis (IPA). B. Prioritized pharmacologic targets in luminal progenitor cells. As a control for our bioinformatic prioritization approach, we chose NF-kB, which was predicted to have low expression in luminal progenitor cells.

Inhibition of Bcl-2 using venetoclax also robustly reduced organoid regeneration (P = 0.0004, 0.002, 0.00005 in biological replicates) (**Figure 5B**). This reduction in regenerative phenotype was mirrored in organoids treated with SB203580, an inhibitor of p38 MAPK, an upstream regulator of Bcl-2 (P = 0.03, 0.005, 0.0008 in biological replicates) (**Figure 5C**) [35]. Due to the combination of predicted downregulation from IPA results as well as the role of NF-kB as a canonical activator of Bcl-2 expression, we used NF-kB as a negative control for our *in vitro* regeneration assay and bioinformatic candidate approach [36]. As predicted, treatment with SC75741, an inhibitor targeting NF-KB, did not significantly reduce the regenerative phenotype of prostate cell organoids (**Figure 5D**). The lack of regenerative phenotype upon treatment with SC75741 supports our candidate selection approach as capable of discerning critical pathways in LPCs.

Targeting prioritized LPC regulators BCL-2 and HIPPO also ablates regeneration in human model systems

Finally, we wanted to investigate whether these drug treatments also ablated the progenitor cell regeneration phenotype using human model systems. Cells from normal regions of human prostates were cultured as organoids as described by McCray et al. [18] Organoids were treated with venetoclax, SB203580, SC75741, or CA3 to test the efficacy of these inhibitors to ablate human progenitor cell regeneration *in vitro*. Treatment with either CA3 (P = 2.3e-8) or venetoclax (P = 5.8e-5) significantly reduced colony formation *in vitro*, similar to that observed in mouse organoids (**Figure 6A**, **6B**). Treatment with negative control SC75741 did not significantly change colony formation, similar to the response observed in mouse organoids. Interestingly, treatment with the p38 MAPK inhibitor SB203580 also did not significantly change colony formation of human cells *in vitro*. This may be due to a differential requirement for p38 MAPK in the survival of human compared to mouse organoids. The reduced regenerative phenotype also was mirrored in average organoid area, providing evidence that the proliferative activity of surviving progenitor cells also was reduced in the presence of CA3 (P = 4.8e-5) and venetoclax (P = 5.8e-5) in human organoids (**Figure 6C**).

Discussion

Here we used scRNA-Seq analysis and bioinformatic prioritization to identify possible mecha-

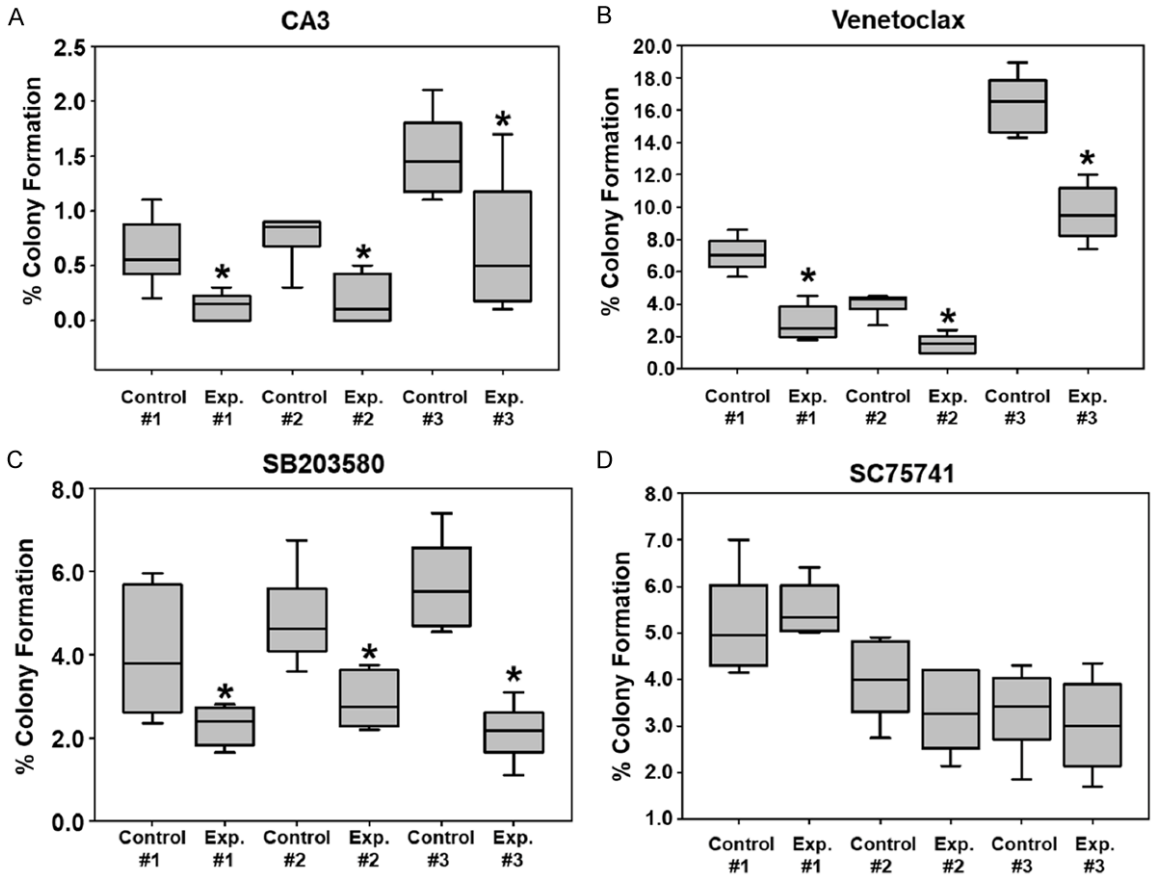

Figure 5. Inhibition of Candidate Factors Inhibits Mouse Prostate Regeneration In Vitro. Quantitation of results for colony forming assays in organoids treated with CA3 (A), venetoclax (B), SB203580 (C), or SC75741 (D). Data represent three sets of organoids from distinct murine hosts and six technical replicates of each set of mouse organoids. *P < 0.05.

nistic vulnerabilities to deplete luminal progenitor cells and pharmacologically target prostate regeneration. We identified and validated the presence of LPCs in both the intact and castrate hormone conditions as expressing the following biomarkers: *Krt8, Krt18, Psca, Tacstd2, Sox2,* and *Tspan8*. scRNA-Seq analysis identified an enrichment of total LPCs in the castrate prostrate, supporting their potential role in regeneration. Additionally, our scRNA-Seq analysis identified luminal diversity in the castrate condition that implies the appearance of intermediate cell populations not present in the intact hormonal condition. Another unique luminal population was found to express *Nkx3.1* while not expressing other putative progenitor cell markers, providing evidence that *Nkx3.1* marks a population separate from LPC populations. Our method of leveraging gene lists generated by Seurat for candidate factors necessary for the LPC phenotype implicated Bcl-2 regulation of apoptosis and the YAP1/HIPPO signaling axis as key factors in maintaining LPCs. Additionally, further investigation of candidate factors upstream of Bcl-2 implies that the activation state of BCL-2 is more important than gene expression. The necessity of both BCL-2 and YAP1 for *in vitro* regeneration phenotypes was validated in human-derived organoids as well, yielding evidence that the effect of these factors upon prostate regeneration phenotypes is reproducible across different species and culture conditions.

Our scRNA-Seq analysis is in accordance with recently published scRNA-Seq analyses from other research groups. Crowell et al. observed an increased number of LPCs in the aging mouse prostate [15]. The genetic markers used in their analysis to denote LPCs significantly

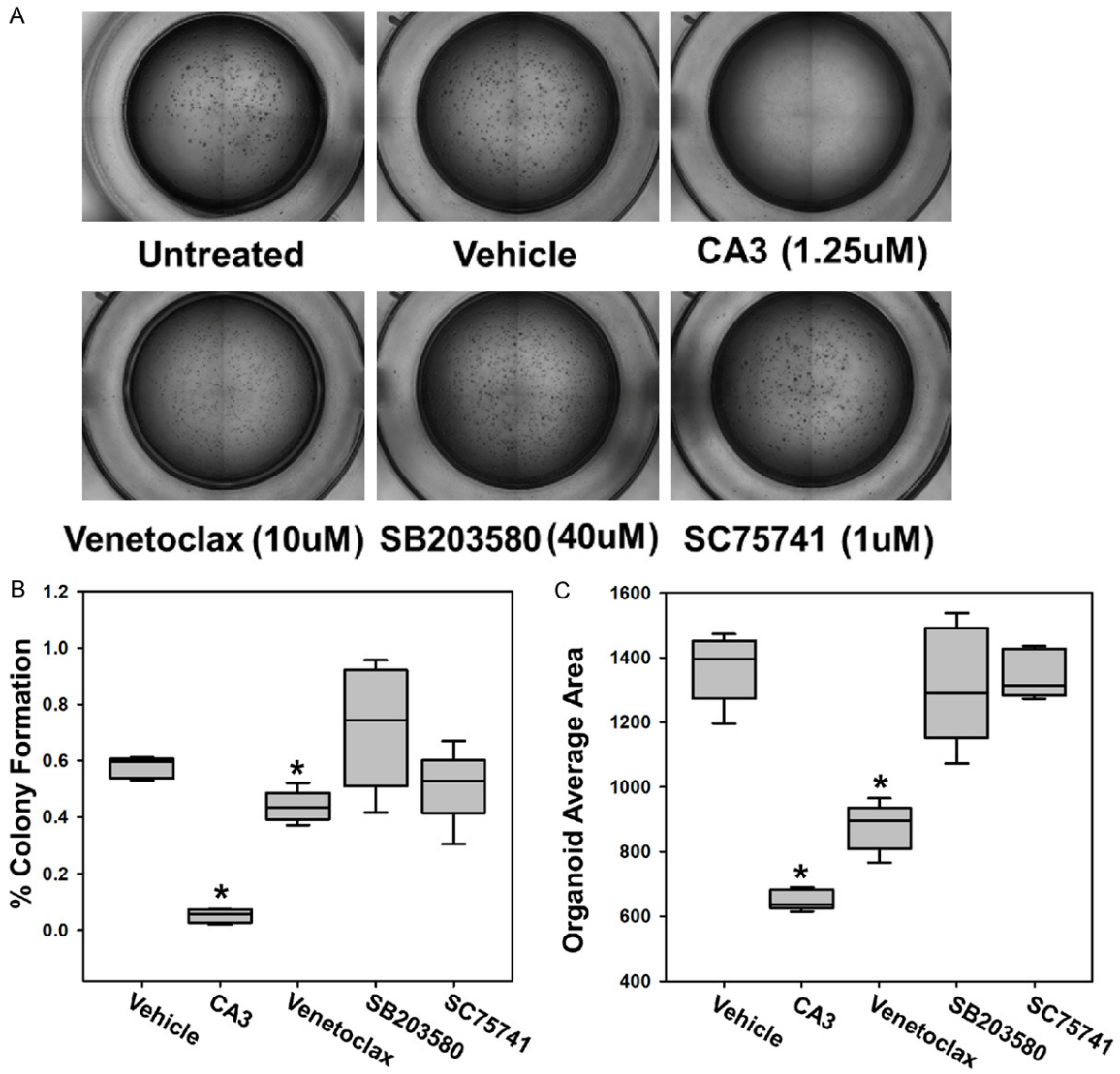

Figure 6. Inhibition of BCL-2 and YAP1 successfully ablate human prostate regeneration in vitro. A. Representative images depicting wells of human prostate organoids treated with drugs at the specified doses. B. Colony-forming assay data comparing the regenerative phenotype of drug-treated human organoids to untreated and vehicle-treated controls. C. Measurements of average organoid area (in pixels), providing an orthogonal measurement of regenerative response in drug-treated and control conditions. *P < 0.05.

overlap with the markers we used, including *Tacstd2, Psca*, and *Krt6a* [15]. Although *Tspan8* was not described as a genetic marker of prostate LPCs in their study, this may be due to minor differences in analysis parameters. Additionally, the study reported expansion in the number of PSCA+ LPCs in the aging process, mirroring our observation of expansion of the LPC population in the castrate prostate [4]. Both of these hormonal contexts are divergent from the hormone-normal environment of the healthy young mouse prostate and are marked by a decrease of androgen signaling [37, 38]. Further, Joseph et al. investigated the mouse prostate epithelium by probing specific locations in the prostate anatomy for a LPC signal. The study identified cells expressing a similar cadre of biomarkers to those outlined in our results, including *Tacstd2, Psca*, and *Krt9* [24]. Joseph et al. also identified the location of LPCs as the proximal ducts next to the prostatic urethra. Due to the similarity in biomarker profiles between our scRNA-Seq analysis and that of Joseph et al., it stands to reason that the LPCs

we identified are localized to the same region of the prostate anatomy.

Finally, Karthaus et al. [16] also observed LPCs in their analysis, reporting similar markers to our analysis and Crowell et al. Additionally, Karthaus et al. acquired mouse samples from multiple time points during prostate involution post-castration and prostate regeneration after reintroduction of androgen. These data indicate an adaptation of stem-like gene expression phenotypes by the luminal cells surviving castration, regardless of their identity before castration [16]. This conclusion provides an explanation for our own observations, as we saw a significant increase in luminal cells expressing *Tacstd2* and other stem markers in the castrate prostate. Karthaus et al. also were able to increase the organoid-forming potential of cells isolated from mouse prostates through the addition of FGF-10, ERG, and NRG to the culture media [16]. This approach is similar to the one we pursued in our analysis, although we tried to ablate cell regeneration *in vitro* with our additions to the organoid media. There is some evidence for overlap between the specific factors targeted in this paper and those targeted by Karthaus et al. For example, Fgf signaling induces a pro-survival effect in target cells and can directly upregulate expression of Bcl family member proteins including BCL-2 in certain contexts [39, 40]. Additionally, certain modalities of YAP1 activity can lead to increased expression of FGF ligands [41]. Altogether, these data imply that our investigation and that of Karthaus et al. could be probing pieces of the same larger network of factors regulating the survival and regeneration phenotypes of prostate epithelial cells. Further investigation is required to understand the full breadth of involved factors and identify specific contributors that are uniquely necessary for the prostate progenitor phenotype.

The drugs we used in our organoid studies have been employed to varying degrees in the prostate context. To date, CA3 has not been used in preliminary studies to treat prostate disease, although the HIPPO pathway contributes to prostate cancer progression, and YAP1 contributes to cancer cell growth and invasion in vitro [33, 42]. Additionally, treatment of TRAMP cancer model mice with verteporfin, a different YAP1 inhibitor, significantly reduces cancer recurrence [43]. Overall, verteporfin is a more commonly used inhibitor of YAP1, but we used CA3 due to its higher specificity in targeting YAP1. Verteporfin has a much lower target affinity for YAP1 compared to CA3, and we chose to use CA3 to avoid decoupling the possible off-target effects of verteporfin from its effect on YAP1 [34]. Although research into YAP1's role in prostate cancer has been extensive, little is known about its role in BPH. Identification of YAP1 as a possible necessary factor in the normal prostate regeneration phenotype warrants potential further investigation of YAP1 in the benign disease context.

Modulation of MAPK signaling has shown promise as a treatment for prostate cancer (PCa), although these pathways have not been investigated as deeply in the context of BPH. SC203580 has been tested *in vitro* on prostate cancer cells in monolayer culture, yielding a decrease in salinomycin-regulated autophagy in cells treated with LY294002 [44]. More broadly, p38 MAPK signaling has been of great interest in the field of prostate disease due to its known dysregulation in PCa as well as data implying possible tumorigenic and tumor suppressor effects of this dysregulation in the PCa context [45]. As of now, this is the first study to test the effectiveness of SB203580 in ablating normal prostate organoid growth *in vitro*. Similarly, NF-kB also has been a target of interest in the field of prostate disease due to its role in the IL-6 signaling pathway and its observed activation in some prostate cancers [46-48]. SC75741 specifically has not been tested in the context of normal prostate regeneration or prostate disease, and in our experience was not effective in reducing organoid regeneration. The BCL-2 axis of apoptosis regulation has been studied extensively in the context of PCa, as this factor contributes to survival of castration-resistant PCa cells [30, 49]. Venetoclax has been used as a therapeutic drug for advanced PCa in mouse models and is currently in clinical trials for human patients [50]. Although venetoclax shows promise as a cancer therapeutic, the role of BCL-2 in BPH and normal prostate regeneration warrants additional investigation. Thus, these data have the potential to help advance study of normal prostate regeneration and also spur interest in testing these factors as possible treatment targets in the context of benign disease and cancer prevention.

Although these data are promising, this study has several shortcomings. First, it is important to note that the inhibitors were not tested in combination, precluding analyses of the interrelatedness of factors as well as factors whose interactions have been validated in other contexts. Second, organoid culture is an *in vitro* facsimile of regeneration and not exactly the same as the physiological phenomenon. Despite that the interplay of specific cell signals and interactions is impossible to perfectly mimic *in vitro*, the organoid context provides a method to induce and measure a regenerative response *in vitro*, and the organoid "tissue" produced in this context exhibits similar epithelial organization to prostate epithelial glands and can undergo involution in response to the removal of androgen similar to the physiological prostate *in vivo* [51]. Thus, additional *in vivo* studies to evaluate the efficacy of our prioritized compounds on murine prostate growth and regeneration are warranted.

Conclusion

Using scRNA-Seq data and unbiased pathway prioritization bioinformatics, we identified two pharmacologic targets that are necessary for prostate organoid regeneration using mouse and human model systems. Further, scRNA-Seq analyses enabled specific targeting of LPC populations that have been implicated in prostate disease initiation and tissue regeneration. Future studies investigating the specificity of such drugs against LPCs and prostate regeneration *in vivo*, along with additional mechanistic and drug discovery approaches, have the potential to identify new treatment modalities to prevent prostate cancer and target BPH.

Acknowledgements

Special thanks to the University of Illinois at Chicago Department of Pathology, including Alan Diamond, Ph.D., Larisa Nonn, Ph.D., and Frederick Behm, M.D., as well as the University of Chicago Committee on Development, Regenerative, and Stem Cell Biology members including Ilaria Rebay, Ph.D., for providing excellent research and training environments. We also thank University of Illinois at Chicago Animal Facilities personnel including Sang Su Oh and Jeanette Purcell for daily animal care and for providing animal surgery facilities. We thank the University of Illinois at Urbana-Champaign Sequencing Core including Alvaro Hernandez, Ph.D., for sequencing services and advice on sample prep and analysis, the University of Illinois at Chicago Research Histology Core for cutting frozen tissue blocks, the University of Illinois at Chicago Bioinformatics Core, and the University of Illinois at Chicago Advanced Cyberstructure for Education Research Core and supercomputing cluster. Lastly, thanks to Gayatry Mohapatra, Ph.D., and her lab for use of the TapeStation during quality control steps of the 10x Genomics library prep workflow. This project was supported by R01-DK124473 (D.J. Vander Griend) and The Pierce Family Foundation; D. Moline was supported by NIH F31DK122746 and NIH T32 GM007183, J. Vellky is supported by the KUH FORWARD Training Program (NIDDK U2CDK129917/TL1-DK132769).

Disclosure of conflict of interest

None.

Address correspondence to: Dr. Donald J Vander Griend, Department of Pathology, The University of Illinois at Chicago, 840 S. Wood Street, 130 CSN, MC 847, Chicago, IL 60612, USA. E-mail: dvanderg@uic.edu

References

[1] Aaron L, Franco OE and Hayward SW. Review of prostate anatomy and embryology and the etiology of benign prostatic hyperplasia. Urol Clin North Am 2016; 43: 279-288.

[2] Ittmann M. Anatomy and histology of the human and murine prostate. Cold Spring Harb Perspect Med 2018; 8: a030346.

[3] Lee CH, Akin-Olugbade O and Kirschenbaum A. Overview of prostate anatomy, histology, and pathology. Endocrinol Metab Clin North Am 2011; 40: 565-575, viii-ix.

[4] Ramsey EW. Benign prostatic hyperplasia: a review. Can J Urol 2000; 7: 1135-1143.

[5] Rawla P. Epidemiology of prostate cancer. World J Oncol 2019; 10: 63-89.

[6] Wei JT, Calhoun E and Jacobsen SJ. Urologic diseases in America project: benign prostatic hyperplasia. J Urol 2005; 173: 1256-1261.

[7] Wang X, Kruithof-de Julio M, Economides KD, Walker D, Yu H, Halili MV, Hu YP, Price SM, Abate-Shen C and Shen MM. A luminal epithelial stem cell that is a cell of origin for prostate cancer. Nature 2009; 461: 495-500.

[8] Goldstein AS, Stoyanova T and Witte ON. Primitive origins of prostate cancer: in vivo evidence

for prostate-regenerating cells and prostate cancer-initiating cells. Mol Oncol 2010; 4: 385-396.
[9] Tokar EJ, Ancrile BB, Cunha GR and Webber MM. Stem/progenitor and intermediate cell types and the origin of human prostate cancer. Differentiation 2005; 73: 463-473.
[10] Sugimura Y, Cunha GR and Donjacour AA. Morphological and histological study of castration-induced degeneration and androgen-induced regeneration in the mouse prostate. Biol Reprod 1986; 34: 973-983.
[11] Cunha GR and Lung B. The possible influence of temporal factors in androgenic responsiveness of urogenital tissue recombinants from wild-type and androgen-insensitive (Tfm) mice. J Exp Zool 1978; 205: 181-193.
[12] Isaacs JT. Antagonistic effect of androgen on prostatic cell death. Prostate 1984; 5: 545-557.
[13] Isaacs JT. Control of cell proliferation and cell death in the normal and neoplastic prostate: a stem cell model. Washington, D.C.; NIH Bethesda, MD: U.S. Dept. of Health and Human Services, Publication #87-2881; 1987.
[14] Tsujimura A, Koikawa Y, Salm S, Takao T, Coetzee S, Moscatelli D, Shapiro E, Lepor H, Sun TT and Wilson EL. Proximal location of mouse prostate epithelial stem cells: a model of prostatic homeostasis. J Cell Biol 2002; 157: 1257-1265.
[15] Crowell PD, Fox JJ, Hashimoto T, Diaz JA, Navarro HI, Henry GH, Feldmar BA, Lowe MG, Garcia AJ, Wu YE, Sajed DP, Strand DW and Goldstein AS. Expansion of luminal progenitor cells in the aging mouse and human prostate. Cell Rep 2019; 28: 1499-1510, e1496.
[16] Karthaus WR, Hofree M, Choi D, Linton EL, Turkekul M, Bejnood A, Carver B, Gopalan A, Abida W, Laudone V, Biton M, Chaudhary O, Xu T, Masilionis I, Manova K, Mazutis L, Pe'er D, Regev A and Sawyers CL. Regenerative potential of prostate luminal cells revealed by single-cell analysis. Science 2020; 368: 497-505.
[17] Michiel Sedelaar JP, Dalrymple SS and Isaacs JT. Of mice and men-warning: intact versus castrated adult male mice as xenograft hosts are equivalent to hypogonadal versus abiraterone treated aging human males, respectively. Prostate 2013; 73: 1316-1325.
[18] McCray T, Moline D, Baumann B, Vander Griend DJ and Nonn L. Single-cell RNA-Seq analysis identifies a putative epithelial stem cell population in human primary prostate cells in monolayer and organoid culture conditions. Am J Clin Exp Urol 2019; 7: 123-138.
[19] Satija R, Farrell JA, Gennert D, Schier AF and Regev A. Spatial reconstruction of single-cell gene expression data. Nat Biotechnol 2015; 33: 495-502.
[20] Drost J, Karthaus WR, Gao D, Driehuis E, Sawyers CL, Chen Y and Clevers H. Organoid culture systems for prostate epithelial and cancer tissue. Nat Protoc 2016; 11: 347-358.
[21] Butler A, Hoffman P, Smibert P, Papalexi E and Satija R. Integrating single-cell transcriptomic data across different conditions, technologies, and species. Nat Biotechnol 2018; 36: 411-420.
[22] Toivanen R, Mohan A and Shen MM. Basal progenitors contribute to repair of the prostate epithelium following induced luminal anoikis. Stem Cell Reports 2016; 6: 660-667.
[23] Goldstein AS, Lawson DA, Cheng D, Sun W, Garraway IP and Witte ON. Trop2 identifies a subpopulation of murine and human prostate basal cells with stem cell characteristics. Proc Natl Acad Sci U S A 2008; 105: 20882-20887.
[24] Joseph DB, Henry GH, Malewska A, Iqbal NS, Ruetten HM, Turco AE, Abler LL, Sandhu SK, Cadena MT, Malladi VS, Reese JC, Mauck RJ, Gahan JC, Hutchinson RC, Roehrborn CG, Baker LA, Vezina CM and Strand DW. Urethral luminal epithelia are castration-insensitive cells of the proximal prostate. Prostate 2020; 80: 872-884.
[25] McAuley E, Moline D, VanOpstall C, Lamperis S, Brown R and Vander Griend DJ. Sox2 expression marks castration-resistant progenitor cells in the adult murine prostate. Stem Cells 2019; 37: 690-700.
[26] Kato M, Ishii K, Iwamoto Y, Sasaki T, Kanda H, Yamada Y, Arima K, Shiraishi T and Sugimura Y. Activation of FGF2-FGFR signaling in the castrated mouse prostate stimulates the proliferation of basal epithelial cells. Biol Reprod 2013; 89: 81.
[27] Kwon OJ, Zhang Y, Li Y, Wei X, Zhang L, Chen R, Creighton CJ and Xin L. Functional heterogeneity of mouse prostate stromal cells revealed by single-cell RNA-Seq. iScience 2019; 13: 328-338.
[28] Lee SH, Johnson DT, Luong R, Yu EJ, Cunha GR, Nusse R and Sun Z. Wnt/beta-catenin-responsive cells in prostatic development and regeneration. Stem Cells 2015; 33: 3356-3367.
[29] Henry GH, Malewska A, Joseph DB, Malladi VS, Lee J, Torrealba J, Mauck RJ, Gahan JC, Raj GV, Roehrborn CG, Hon GC, MacConmara MP, Reese JC, Hutchinson RC, Vezina CM and Strand DW. A cellular anatomy of the normal adult human prostate and prostatic urethra. Cell Rep 2018; 25: 3530-3542, e3535.
[30] Kelly PN and Strasser A. The role of Bcl-2 and its pro-survival relatives in tumourigenesis and cancer therapy. Cell Death Differ 2011; 18: 1414-1424.
[31] Kwon OJ, Valdez JM, Zhang L, Zhang B, Wei X, Su Q, Ittmann MM, Creighton CJ and Xin L. Increased Notch signalling inhibits anoikis and

stimulates proliferation of prostate luminal epithelial cells. Nat Commun 2014; 5: 4416.
[32] Peng YC and Joyner AL. Hedgehog signaling in prostate epithelial-mesenchymal growth regulation. Dev Biol 2015; 400: 94-104.
[33] Salem O and Hansen CG. The hippo pathway in prostate cancer. Cells 2019; 8: 370.
[34] Song S, Xie M, Scott AW, Jin J, Ma L, Dong X, Skinner HD, Johnson RL, Ding S and Ajani JA. A novel YAP1 inhibitor targets CSC-enriched radiation-resistant cells and exerts strong antitumor activity in esophageal adenocarcinoma. Mol Cancer Ther 2018; 17: 443-454.
[35] De Chiara G, Marcocci ME, Torcia M, Lucibello M, Rosini P, Bonini P, Higashimoto Y, Damonte G, Armirotti A, Amodei S, Palamara AT, Russo T, Garaci E and Cozzolino F. Bcl-2 phosphorylation by p38 MAPK: identification of target sites and biologic consequences. J Biol Chem 2006; 281: 21353-21361.
[36] Catz SD and Johnson JL. Transcriptional regulation of bcl-2 by nuclear factor kappa B and its significance in prostate cancer. Oncogene 2001; 20: 7342-7351.
[37] Liu TT, Thomas S, McLean DT, Roldan-Alzate A, Hernando D, Ricke EA and Ricke WA. Prostate enlargement and altered urinary function are part of the aging process. Aging (Albany NY) 2019; 11: 2653-2669.
[38] Nicholson TM and Ricke WA. Androgens and estrogens in benign prostatic hyperplasia: past, present and future. Differentiation 2011; 82: 184-199.
[39] Agas D, Marchetti L, Menghi G, Materazzi S, Materazzi G, Capacchietti M, Hurley MM and Sabbieti MG. Anti-apoptotic Bcl-2 enhancing requires FGF-2/FGF receptor 1 binding in mouse osteoblasts. J Cell Physiol 2008; 214: 145-152.
[40] Ornitz DM and Itoh N. The fibroblast growth factor signaling pathway. Wiley Interdiscip Rev Dev Biol 2015; 4: 215-266.
[41] Zhao B, Wei X, Li W, Udan RS, Yang Q, Kim J, Xie J, Ikenoue T, Yu J, Li L, Zheng P, Ye K, Chinnaiyan A, Halder G, Lai ZC and Guan KL. Inactivation of YAP oncoprotein by the Hippo pathway is involved in cell contact inhibition and tissue growth control. Genes Dev 2007; 21: 2747-2761.
[42] Kuser-Abali G, Alptekin A, Lewis M, Garraway IP and Cinar B. YAP1 and AR interactions contribute to the switch from androgen-dependent to castration-resistant growth in prostate cancer. Nat Commun 2015; 6: 8126.
[43] Jiang N, Ke B, Hjort-Jensen K, Iglesias-Gato D, Wang Z, Chang P, Zhao Y, Niu X, Wu T, Peng B, Jiang M, Li X, Shang Z, Wang Q, Chang C, Flores-Morales A and Niu Y. YAP1 regulates prostate cancer stem cell-like characteristics to promote castration resistant growth. Oncotarget 2017; 8: 115054-115067.
[44] Kim KY, Park KI, Kim SH, Yu SN, Park SG, Kim YW, Seo YK, Ma JY and Ahn SC. Inhibition of autophagy promotes salinomycin-induced apoptosis via reactive oxygen species-mediated PI3K/AKT/mTOR and ERK/p38 MAPK-dependent signaling in human prostate cancer cells. Int J Mol Sci 2017; 18: 1088.
[45] Koul HK, Pal M and Koul S. Role of p38 MAP kinase signal transduction in solid tumors. Genes Cancer 2013; 4: 342-359.
[46] Paule B, Terry S, Kheuang L, Soyeux P, Vacherot F and de la Taille A. The NF-kappaB/IL-6 pathway in metastatic androgen-independent prostate cancer: new therapeutic approaches? World J Urol 2007; 25: 477-489.
[47] Suh J and Rabson AB. NF-kappaB activation in human prostate cancer: important mediator or epiphenomenon? J Cell Biochem 2004; 91: 100-117.
[48] Torrealba N, Vera R, Fraile B, Martinez-Onsurbe P, Paniagua R and Royuela M. TGF-beta/PI3K/AKT/mTOR/NF-kB pathway. Clinicopathological features in prostate cancer. Aging Male 2020; 23: 801-811.
[49] Kim JH, Lee H, Shin EA, Kim DH, Choi JB and Kim SH. Implications of Bcl-2 and its interplay with other molecules and signaling pathways in prostate cancer progression. Expert Opin Ther Targets 2017; 21: 911-920.
[50] Suvarna V, Singh V and Murahari M. Current overview on the clinical update of Bcl-2 anti-apoptotic inhibitors for cancer therapy. Eur J Pharmacol 2019; 862: 172655.
[51] Karthaus WR, Iaquinta PJ, Drost J, Gracanin A, van Boxtel R, Wongvipat J, Dowling CM, Gao D, Begthel H, Sachs N, Vries RGJ, Cuppen E, Chen Y, Sawyers CL and Clevers HC. Identification of multipotent luminal progenitor cells in human prostate organoid cultures. Cell 2014; 159: 163-175.

Supplementary Table 1. Antibodies Used for Immunofluorescence and Flow Cytometry

TARGET PROTEIN	Host Organism	Manufacturer	Dilution
CD26	Rat	Biolegend (San Diego, CA)	1 ug/million cells
PSCA	Rabbit	Lifespan Biosciences (Seattle, WA)	1:100 (Tissue) 1:100 (Organoids)
TSPAN8	Rat	R&D Biosystems (Minneapolis, MN)	1:50 (Tissue) 1:100 (Organoids)
TSPAN8 (PE-Conjugated)	Rat	R&D Biosystems	10 uL/million cells
KRT5	Chicken	Biolegend	1:1000 (Tissue) 1:100 (Organoids)

Supplementary Table 2. Quality Control Metrics for Mouse Prostate Samples and scRNA-Seq Analyses

READOUT	Intact	Castrate
Viability at Collection	80.2%	74.2%
Sample Density	5.12e6 cells/mL	2.59e5 cells/mL
Average Features Per Cell	989.78	1401.37
Number of Principle Components	43	43
Modularity of Generated UMAP	0.8412	0.8902

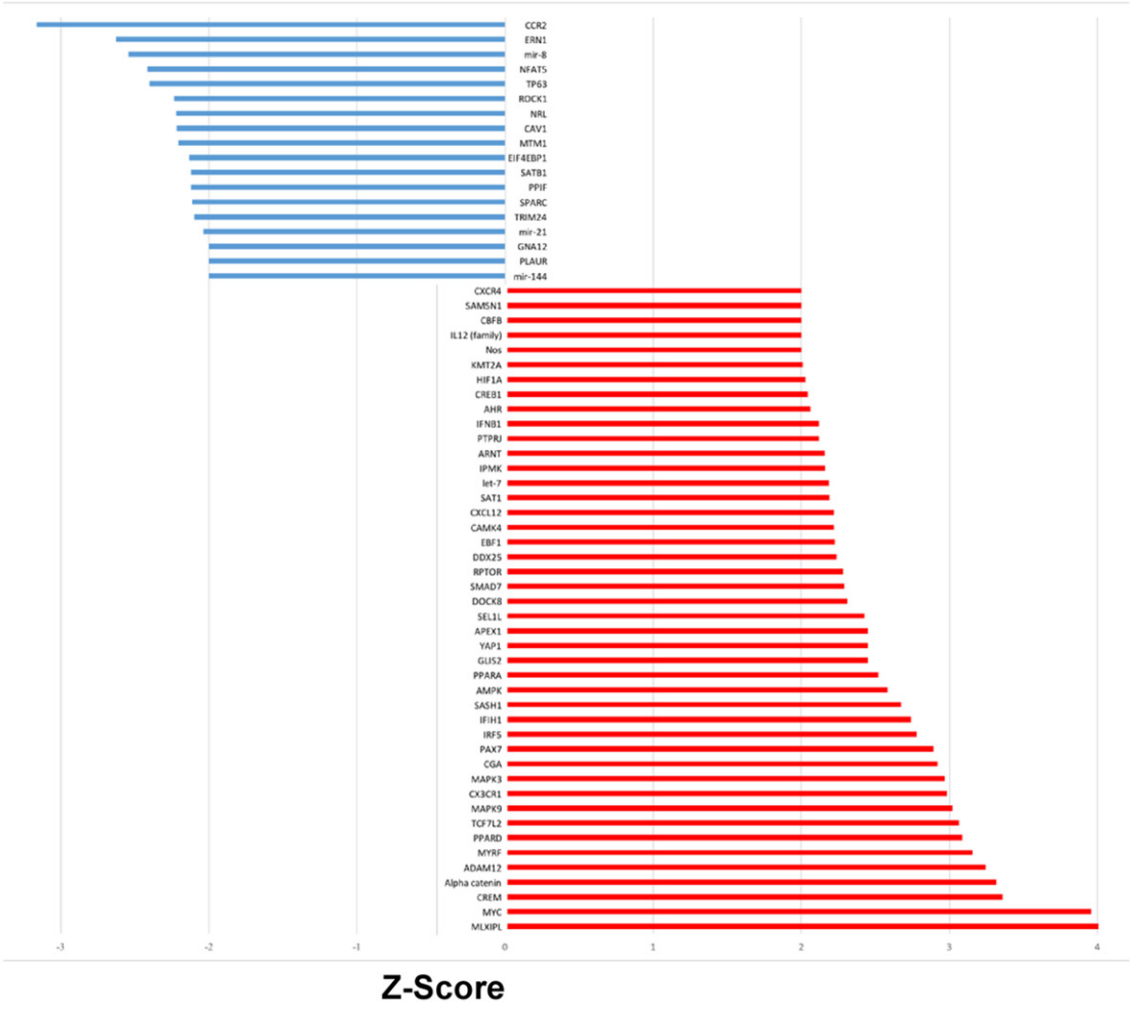

Supplementary Figure 1. Upstream regulator analysis of luminal progenitor cells. Upstream regulator analysis identified candidate factors predicted to have an effect in luminal progenitor cell-specific pathways. Factors of interest in upstream analysis include YAP1 and upstream regulators of BCL-2 including IL12, HIF1A, ARNT, and MAPK9.